

Wide cylindrical or spherical optical potentials from laser beam superpositions

Ole Steuernagel

*School of Physics, Astronomy and Mathematics,
University of Hertfordshire, Hatfield, AL10 9AB, UK **

(Dated: November 20, 2018)

Abstract

Superpositions of paraxial Laguerre-Gauss laser beam modes to generate optical potentials based on the optical dipole force are investigated theoretically. Parabolic and other monomial potentials with even powers, in cylindrical and spherical symmetry, with large diameters, can be synthesized. This superposition approach promises to help with high quality atom cloud manipulation and imaging.

PACS numbers: 32.80.Lg, 32.80.Qk, 42.50.Vk, 42.60.Jf

arXiv:0904.4342v1 [physics.optics] 28 Apr 2009

*Electronic address: O.Steuernagel@herts.ac.uk

I. INTRODUCTION

The fields of atom [1] and molecular optics [2, 3] have developed considerably over recent years. Atomic beams that behave like laser beams can be created [4]; they are considered for direct deposition [1], used in microscopy [5], precision metrology [6], and for the studies of quantum statistical effects [7, 8] such as the Hanbury Brown-Twiss effect [9].

The quality of the preparation of atomic ensembles, particularly in the cases of ultracold gases, is excellent, frequently as good as fundamental limits allow [10, 11]. The same is not true of atom-optical components, for example atom-beam focussing [1] suffers from the lack of lenses with large numerical apertures, see [12] and references therein. Similarly, wide parabolic optical dipole potentials for focussing and defocussing [9] of atomic clouds at tolerable laser beam power [12, 13] are currently unavailable.

Here, the use of the optical dipole force for the application of wide high-quality aberration-free pulsed or stationary 2D and 3D isotropic potentials, primarily for the manipulation of cold gas clouds, is considered. In the regime of laser light far detuned from the atomic transition the resulting potentials are conservative and their strength is proportional to the laser light intensity [1, 14]. It is shown that superpositions of Laguerre-Gaussian beams using spatial light modulators allow us to tailor laser beams in a suitable fashion [15] to create wide cylindrical and spherical optical potentials improving control for the manipulation of atomic or molecular clouds. Harmonic potentials are considered in greatest detail because of their importance for focussing [12] and defocussing [9, 12] in atom optics and atomic lithography [1] or for feeding into waveguides [13] of atomic chips [16]. The superposition approach can be extended to non-harmonic potentials with cylindrical and spherical symmetry, see section III below. Non-harmonic potentials should facilitate dynamical studies of trapped atom clouds [17], perturbations, the formation of caustics, and aspects of quantum-classical behaviour [18].

For focussing and defocussing of atomic beams many approaches have been investigated, see references in [12]. For focussing and defocussing of cold gas clouds in two and three dimensions magnetic focussing [19, 20, 21, 22] setups have been experimentally implemented [13]. When miniaturizing such approaches care has to be taken that unwanted interactions with bulk media do not disturb trapped gas [23]. The superposition approach introduced here is meant to complement these and make the great flexibility of optical dipole

force approaches more accessible.

In section II we briefly recap the physics of Laguerre-Gauss modes $LG_{p,l}$ and the optical dipole force. We find that superpositions of members of the family $\{LG_{p,1}, p = 0, \dots, N_{max}\}$ are required for the generation of parabolic potentials, other values of orbital angular momentum l can yield purely monomial potentials of order $2l$. We determine the expansion coefficients needed to create the desired optical potentials with cylindrical symmetry in section III. An important consequence of the superposition approach and the main motivation for this work is the ability to very considerably save laser power, see subsection III C. Wide aberration-free optical dipole force potentials become realizable which currently are infeasible because of laser beam dilution, this has been recognized as a road block for some time: “In spite of numerous impressive achievements, using laser light interaction to tailor atom beams demands a high quality of the transverse collimation and this technique is difficult to scale with accessible laser powers” [13].

The use of Laguerre-Gauss beams is not only experimentally well established [24] they also form an appropriate basis for our analysis: limitations of the superposition approach arise because of mode-dispersion due to Gouy’s phase [12, 25]. This phase is incorporated in the definition of Laguerre-Gauss modes, see Eq. (1); its effects are considered in subsections III D and IV A. We finally show how crossing two modulated beams with cylindrical symmetry can be used to form a spherically symmetrical potential in section IV and conclude in section V.

II. LAGUERRE-GAUSS BEAMS

Laguerre-Gauss modes are monochromatic, paraxial beam solutions [25, 26, 27, 28, 29] and are defined as

$$\begin{aligned}
 LG(p, l, z_R, \lambda_L, \rho, z) = & \sqrt{\frac{2}{(1 + \delta_{0l})\pi} \frac{p!}{(p+l)!}} \left(\frac{\sqrt{2} \rho}{w(z)} \right)^l L\left(p, l, 2 \frac{\rho^2}{w(z)^2}\right) \\
 & \times \left(\frac{e^{i l \xi}}{w(z)} \right) e^{-\frac{\rho^2}{w(z)^2}} e^{-i(2p+l+1)\phi(z)} e^{\frac{i k_L \rho^2}{2R(z)}}. \quad (1)
 \end{aligned}$$

Here, the monochromatic plane wave factor $\exp[i(k_L z - \omega_L t)]$ is omitted [25, 26, 27, 28, 29], L are generalized Laguerre polynomials, p and l the integer valued nodal, and angular momentum numbers respectively, $\mathbf{r} = (\boldsymbol{\rho}, z)$ is the position vector with the transverse coordinate vector $\boldsymbol{\rho} = (x, y)$; the Kronecker-delta function δ_{0l} reflects the fact that the modes

with zero angular momentum have to be normalized differently to the other modes. The transverse coordinates also parameterize the orbital angular momentum phase ξ via the relationship $e^{i\xi} = x + iy$ [26]. The frequency of the monochromatic laser ω_L gives rise to its wavenumber $k_L = \omega_L/c = 2\pi/\lambda_L$ where λ_L is the laser light's wavelength. The wave front radii $R(z) = (z^2 + z_R^2)/z$, the beam radii $w(z) = w_0\sqrt{1 + z^2/z_R^2}$, with the focal beam radius $w_0 = \sqrt{\lambda_L z_R/\pi}$, and the longitudinal Gouy-phase shifts $\phi(z) = \arctan(z/z_R)$ are all parameterized by the beams' Rayleigh lengths z_R [26, 27, 28, 29].

Correctly chosen superpositions of modes using spatial light modulators [12, 15, 30]

$$\Psi_P(\mathbf{r}) = \sum_{p=1}^P c_{Pp} \cdot LG(p-1, 1, z_R, \lambda_L, \rho, z) \quad (2)$$

allows us to create superpositions Ψ which give rise to parabolic intensity distributions. Following reference [28] the use of (y -) polarized modes in Equation (2)) yields an electric field which is polarized in the y -direction with a small contribution in the z -direction due to the tilt of wave fronts off the beam axis ($\hat{\mathbf{x}}, \hat{\mathbf{y}}, \hat{\mathbf{z}}$ are the unit-vectors and \Re stands for real-part)

$$\mathbf{E}_P(\mathbf{r}; t) = \Re\{[\hat{\mathbf{y}} \omega_L \Psi_P + \hat{\mathbf{z}} ic \frac{\partial \Psi_P}{\partial x}]e^{i(k_L z - \omega_L t)}\}. \quad (3)$$

In keeping with the paraxial approximation of not overly focussed beams we neglect the transverse derivative in eq. (3). The associated time-averaged light intensity distribution then has the form [28]

$$I_P(\mathbf{r}) = \epsilon_0 \langle \mathbf{E}_P(\mathbf{r}, t)^2 \rangle \approx \frac{\epsilon_0}{2} \omega_L^2 |\Psi_P(\mathbf{r})|^2. \quad (4)$$

A. Normalization, Intensity Scaling and Gradient Reduction

With the normalized modes of Eq. (1) and assuming that the sum of the coefficients $\sum |c_p|^2$ in Eq. (2) is normalized to unity we use the cross-sectional beam power normalization

$$\int_{-\infty}^{\infty} \int_{-\infty}^{\infty} dx dy |\Psi_P(x, y, z)|^2 = \frac{2}{\epsilon_0 \omega_L^2} \int_{-\infty}^{\infty} \int_{-\infty}^{\infty} dx dy I_P(x, y, z) \doteq \frac{2}{\epsilon_0 \omega_L^2} \bar{I}_P = 1. \quad (5)$$

We note that the intensity $I(x, y, z)$ of beams of fixed total power reduces inversely proportionally to their width w_0 in one direction, that is, their field amplitudes scale with $w_0^{-1/2}$ in x and y . Furthermore the field gradients diminish with w_0^{-1} . This implies that the effective curvature of the integrated laser light intensity $\frac{1}{2} \int_0^R |\nabla \Psi|^2 2\pi r dr$, responsible for atomic focussing, scales with w_0^{-4} . We face an unfavourable quartic scaling with the beam width if we attempt to expand a laser beam transversally in ρ in order to widen the effective potential without weakening its power. Additionally, as we will show below, pure modes have small useful areas to generate the desired potentials, the combination of these two factors makes a pure mode approach unfeasible [12, 13, 31]. It forces us to employ the mode superpositions studied here. Below, we discuss two approaches for the compensation of gradient weakening: by power compensation in subsection III A, and by beam waist narrowing in subsection III B.

B. Optical Dipole Force

We assume that the interaction between atoms and the laser light is well described by a two-level scheme (excited state e and ground state g) in rotating wave approximation with effective atomic line width Γ and resonance frequency $\omega = \omega_e - \omega_g$. This leads to the expression $I(\mathbf{r}) \Gamma^2 / (2I_S) = \Omega(\mathbf{r})^2$ for the Rabi-frequency Ω as a function of the ratio of the local laser intensity $I(\mathbf{r})$ and the transition's saturation intensity $I_S = \pi \hbar c \Gamma / (3\lambda^3)$ [14, 32]. With sufficiently weak laser intensity I and sufficiently large detuning $\delta_\omega = \omega_L - \omega$ of the laser frequency ω_L from the atomic transition frequency ω , the AC-Stark shift gives rise to a conservative optical dipole potential which, to first order in I/I_S , has the form [14, 33]

$$U_\omega \approx \frac{\hbar \Gamma^2 I(\mathbf{r})}{8 \delta_\omega I_S} \approx \frac{\epsilon_0 \hbar \Gamma^2 \omega_L^2}{16 \delta_\omega I_S} |\Psi_P(\mathbf{r})|^2. \quad (6)$$

This potential is modified due to detrimental spontaneous emission noise and light fluctuations. These tend to increase with increasing laser intensity but can be decreased by increased detuning [14] or through the use of more complicated optical level schemes [33]. Further discussion of their influences is beyond the scope of this paper.

C. Potentials of order $2l$

We now consider cylindrical atom-potentials with purely monomial modulation in the transverse direction $\propto \rho^{2l}$. A Taylor-expansion in ρ shows that LG -modes with angular

orbital momentum l depend in leading order on ρ^l and every other higher order (ρ^{l+2n} , n a positive integer). The Taylor coefficients of different modes are linearly independent of each other. Combining them into suitable superpositions created from mode families $\{LG_{p,l}, p = 0, \dots, N_{max}\}$ allows us to retain the leading and remove all higher order terms up to and including that of order $\rho^{l+2N_{max}}$. Almost purely monomial potentials of order $2l$ therefore arise from such superpositions.

III. CYLINDRICAL POTENTIALS

The coefficients for superpositions using the mode family $LG_{p,1}$ are straightforward to determine through Gauss elimination. The first six superpositions $\{\Psi_P, P = 1, \dots, 6\}$ yield the following (normalized $\sum_{p=1}^P |c_{Pp}|^2 = 1$) coefficient matrix

$$[c_{Pp}] = \begin{bmatrix} 1.0 & 0.0 & 0.0 & 0.0 & 0.0 & 0.0 \\ 0.9427 & -0.3333 & 0.0 & 0.0 & 0.0 & 0.0 \\ 0.8339 & -0.5360 & 0.1313 & 0.0 & 0.0 & 0.0 \\ 0.7212 & -0.6277 & 0.2883 & -0.05546 & 0.0 & 0.0 \\ 0.6209 & -0.6467 & 0.4150 & -0.1525 & 0.02435 & 0.0 \\ 0.5368 & -0.6261 & 0.4959 & -0.2595 & 0.08003 & -0.01095 \end{bmatrix}. \quad (7)$$

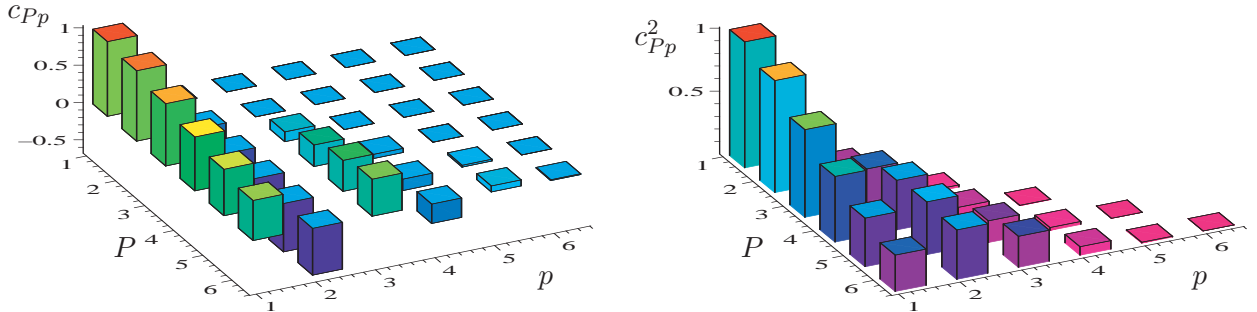


FIG. 1: Amplitude coefficients c_{Pp} and probabilities c_{Pp}^2 of Laguerre-Gauss superpositions Ψ_P of up to $N_{max} = 5^{\text{th}}$ order modes ($P = N_{max} + 1 = 1, 2, \dots, 6$) according to the coefficient matrix (7).

Mode-superpositions extend the “useful” linear part of the field profile yielding wider parabolic intensity profiles. Figures 2 and 3 demonstrate that the parabolic part in the focal intensity profile of a superpositions field grows with the number of modes used.

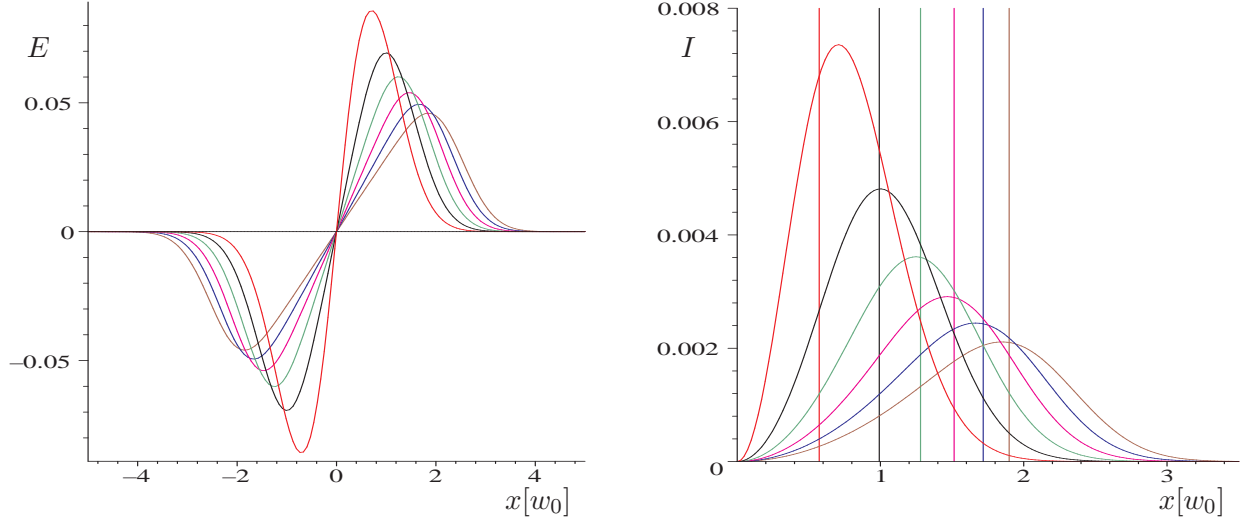


FIG. 2: Left: Transverse electric field profile, $E_P(x, 0, 0)$, and Right: transverse intensity profiles $I_P(x, 0, 0)$ at focal cross-section of Laguerre-Gauss beams comprising superpositions Ψ_P , ($P = 1, \dots, 6$), according to coefficient matrix (7) (x -axis in units of focal beam radius w_0 , total cross-sectional beam power normalized to unity, ($\epsilon_0 \omega_L^2 / 2$ set to unity), Rayleigh lengths z_R kept constant). The vertical bars mark in the plot on the right are located at positions $0.57 \cdot \sqrt{2P+1} \cdot w_{0x}$ confirming harmonic oscillator-scaling [25] of the superposition beams' widths.

A. Increased Beam Powers Compensate for Potentials' Widening

If we increase the total cross-sectional beam power \bar{I}_P for wider beam profiles according to the ratios of the modes' transverse derivatives, $\bar{I}_P \doteq \bar{I}_1 |\partial_x \Psi_1(x, 0, 0) / \partial_x \Psi_P(x, 0, 0)|^2$, the weakened gradient is power-compensated for by increased laser power. This way all superpositions give rise to potentials with equal strength, see Fig. 3, the necessary beam power increase to achieve this compensation is sketched in the inset of Fig. 3.

B. Decreased Rayleigh-Lengths Compensate for Potentials' Widening

Alternatively to the beam-power increases just discussed, we can keep the total beam power for all beams equal and shrink the higher-order superposition-beams' Rayleigh lengths through increased beam focussing in the ρ -direction. This Rayleigh length-matching also allows us to compensate for the gradient reduction observed in Fig. 2. The laser intensity profiles for Rayleigh-matched superpositions are displayed in Fig. 4, the filled-in areas in this figure are limited by the points d_P , where each intensity curve deviates from the enveloping

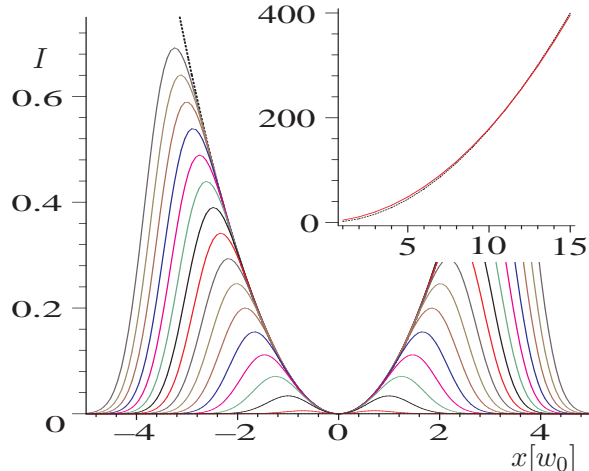


FIG. 3: Focal intensity profiles $I(x, 0)$ of Laguerre-Gauss beam superpositions comprising up to 16th order modes (same units as in Fig. 2). For the superposition modes depicted in the left panel the total beam power has been adjusted such that all profiles have the same curvature at the origin as the dotted line parabola. The inset shows the necessary relative power increase, \bar{I}_P/\bar{I}_1 , as a function of superposition order P (solid red line); it scales approximately like $\frac{16}{9} \cdot P^2$ (inset: dotted black line).

parabola (dotted line) by 0.74 percent. They delineate the useful areas of the potentials. This quality-criterion is adopted from Gallatin and Gould’s work [31] which showed that beyond a deviation of 0.74% spherical aberrations distort the atomic point-spread function of an imaged atomic beam too severely; for more details see references [12] and [31].

C. Power Savings

The filled-in areas in Fig. 4 represent the laser power fraction contributing to the atom potential in each case. Higher-order superpositions clearly allow us to use the laser power much more efficiently. Most of the laser power is wasted in the wings if the superposition approach is not employed. Additionally to the quantification of the useful area of the potentials delineated by the deviation points d_P (see Fig. 4 and Table I). This waste is meaningfully quantified through the determination of the fraction of power \mathcal{E}_P the laser beam contributes to the ‘useful’ part of the potential profile. We define it as the ratio of the laser energy contributing to the area between the deviation points $|\rho| < d_P$, in terms of the total laser power, namely

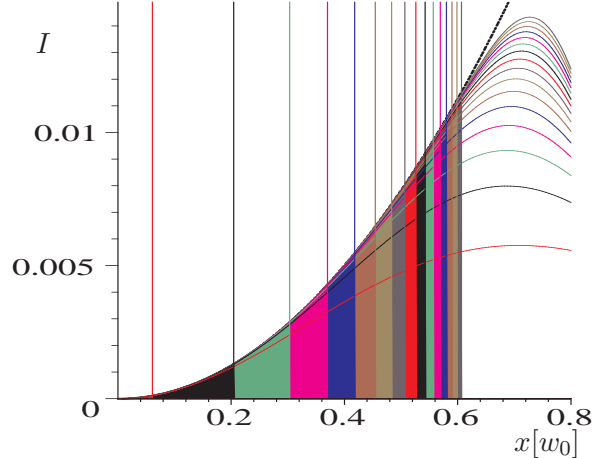


FIG. 4: Focal intensity profiles $I(x,0,0)$ of Laguerre-Gauss beams comprising up to 16th order modes and their 0.74%-deviation marks d_P , which lie at relative positions $d_P/d_1 = 1.00, 3.36, \dots, 9.96$ from the origin, compare Table I (same units as in Fig. 2). In contrast to Fig. 3 all superpositions have the same total beam power \bar{I} , but the Rayleigh lengths z_R have been readjusted such that all higher-order superpositions match up with curvature of the first mode case Ψ_1 , see text.

TABLE I: Potential Parameters d_P and \mathcal{E}_P , compare Fig.4

P	1	2	3	4	5	6	7	8	9	10	11	12	13	14	15	16
d_P/d_1	1.00	3.36	4.98	6.07	6.86	7.46	7.93	8.31	8.63	8.90	9.14	9.34	9.52	9.68	9.83	9.96
\mathcal{E}_P [%]	0.0027	0.35	1.7	3.7	6.1	8.5	11	13	15	17	19	21	23	24	26	27
$\mathcal{E}_P/\mathcal{E}_1$	1	127	614	1362	2221	3103	3967	4791	5570	6306	6991	7639	8244	8816	9352	9858

$$\mathcal{E}_P = \frac{\int_0^{d_P} d\rho \int_0^{2\pi} d\tau I_P(\rho \cos(\tau), \rho \sin(\tau), 0)}{\int_{-\infty}^{\infty} dy \int_{-\infty}^{\infty} dx I_P(x, y, 0)}. \quad (8)$$

Table I and Fig. 5 summarize and quantify our findings: Table I allows us to compare values for a single-mode atom potential, for which $\mathcal{E}_1 = 0.0027\%$, with the superposition approach. For example, compared to mode $\Psi_1 = LG_{0,1}$ the relative power savings in case of superposition Ψ_{16} is 9858, this translates into a power utilization of $\mathcal{E}_{16} = 0.0027\% \times 9858 = 27\%$. In general the details of this behaviour depend on the chosen quality criterion but the underlying scaling is straightforward to derive. The useful fraction of the laser beam is proportional to a 2D integral over the intensity and therefore grows with the fourth power

of the position of the deviation mark $\mathcal{E}_P/\mathcal{E}_1 = (d_P/d_1)^4$, for example $\mathcal{E}_{16}/\mathcal{E}_1 = (d_{16}/d_1)^4 \approx 9.96^4 \approx 9858$.

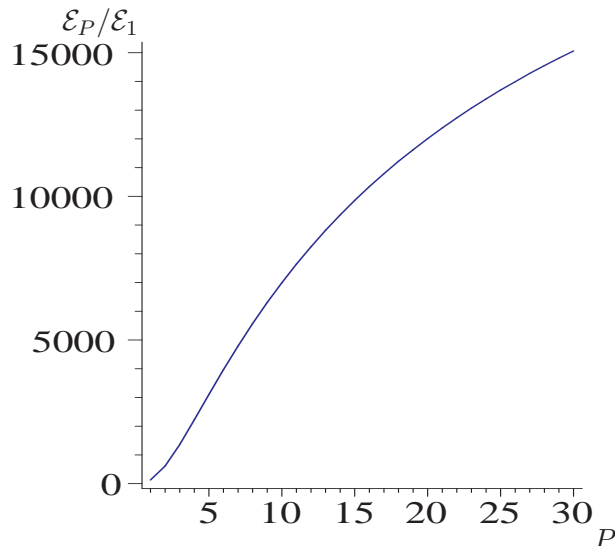


FIG. 5: Relative power savings $\mathcal{E}_P/\mathcal{E}_1$ as a function of superposition mode number P .

D. Limitations due to Mode Dispersion

Different order modes carry different Gouy-phase factors which leads to mode dispersion in the focal region [25]. The associated change in intensity distribution is illustrated in Fig. 6. An interesting case is the creation of spherically symmetrical potentials using two beams with cylindrical symmetry and equal foci orthogonally crossing each other. In this case the width of one beam dictates the area along the beam axis of the other beam that is used. This implies constraints on the degrees of permissible focussing which we investigate in the following section.

IV. SPHERICAL POTENTIALS

We now want to investigate the scenario for the generation of spherically symmetrical potentials. If an identical copy of the laser beam that travels along the z -axis is additionally sent along the x -axis such that their crossed confocal configuration leads to the simultaneous application of two cylindrical potentials a spherical potential is applied to the gas cloud. The laser beams have to be sufficiently detuned from each other in order to avoid harmful

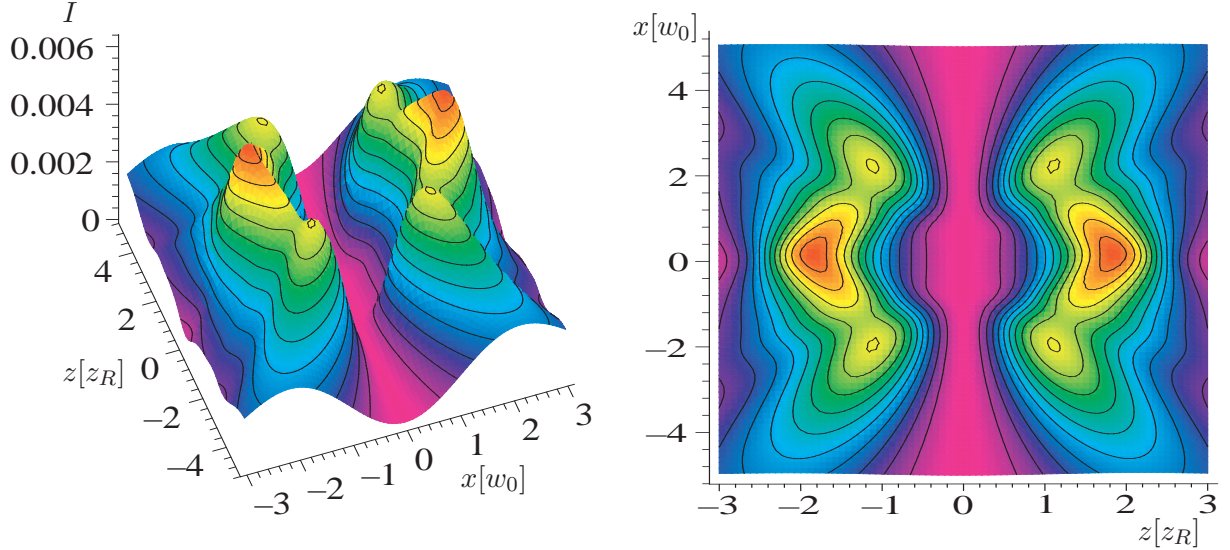


FIG. 6: Intensity profile $I_6(x, 0, z)$ of Laguerre-Gauss superposition Ψ_6 , from two perspectives. The mode dispersive effects of Gouy's phase change the intensity distribution along the beam axis. Note that the x -axis is displayed in terms of the focal beam radius w_0 whereas the z -axis is represented in terms of the Rayleigh length z_R .

interference despite their spatial overlap [34]. They moreover have to be elliptically stretched in the y -direction, by a factor $\sqrt{2}$ in the parabolic case or by $2^{1/(2l)}$ in the case of a monomial potential $\propto \rho^{2l}$, otherwise adding up their intensities would remove the desired isotropy of the spherical potential.

A. Limitations due to Mode Dispersion

Gouy's phase $\phi(z) = \arctan(z/z_R) \approx z/z_R$, varies strongest near the beam focus and introduces relative phases between the modes within each beam [25]. If the beam is very strongly focussed (small value of z_R) the dephasing away from the focus $z = 0$ is so rapid that non-linear aberrations degrade the desired linear field profile. In other words, a lower limit for the Rayleigh lengths $z_{\min}(P)$ as a function of the number of used modes P has to be determined in order to guarantee moderate dephasing. Whereas the absolute values for this lower limit are hard to derive from first principles, we can still work out the correct scaling with the maximal mode number P :

The electric field is proportional to the superposition of the modes including the Gouy-phase factors; this can be approximated by $E_P \propto \sum_{p=0}^{P-1} c_{p+1} LG_p e^{2ip\phi} \approx \sum_{p=0}^{P-1} c_{p+1} LG_p (1 +$

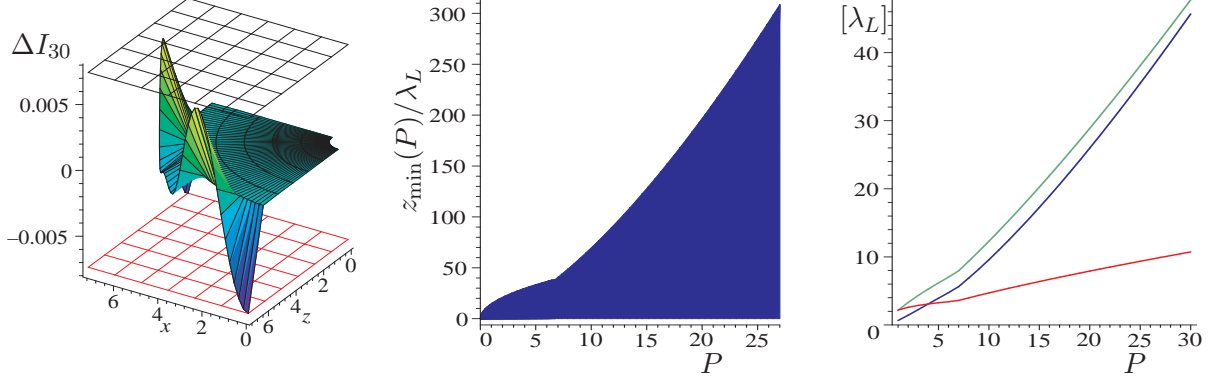


FIG. 7: The left panel illustrates the behavior of the relative deviation of the intensity distribution ΔI from zero as it approaches the 0.74%-deviation marks (top and bottom grid). Here, ΔI_{30} is shown for the crossed configuration of two laser beams travelling along z and x -axis respectively. The value of the Rayleigh length z_R at which we find that the oscillatory behaviour of ΔI along a constant radial perimeter just exhausts the upper and lower limits set by the deviation marks allows us to determine the associated value of z_{\min} . The latter is plotted as a function of maximum mode number, in the middle panel (the filled in blue area is the forbidden area of too tightly focussed beams). The values of $z_{\min}(P)$ in turn determine the position of the turning points $0.57 \cdot \sqrt{2P+1} \cdot w_0$ (top green line, compare Fig. 2), the position of the deviation-points d_P (middle blue line), and the focal beam radii $w_0(z_{\min}(P))$ (lower red line), depicted in terms of the laser's wavelength λ_L in the right panel.

$2ipz/z_R$). The expansion coefficients are positive and the wave functions are real at the focus $z = 0$. Since the first order term is purely imaginary the intensity has to depend on z quadratically: $I_P(x, y, z) = I_P(x, y, 0) \cdot [1 + \frac{z^2}{z_R^2} D_P + \mathcal{O}(z^4)]$. The deviation term D_P has a complicated dependence on the number of modes, but, containing the square of sums of the form $\sum_{p=0}^{P-1} p c_{p+1} L G_p$, is roughly proportional to P^2 . When we consider the relative deviation of the intensity profile near the focus from the focal intensity distribution, $\Delta I = \frac{I(z) - I(0)}{I(0)}$, we find $\Delta I_P \propto \frac{z^2}{z_R^2} \cdot P^2$. Additionally, we know that the widths of the superpositions scale roughly like those of the harmonic oscillator [25], see Fig. 2, namely $z \propto \sqrt{2P+1} \approx \sqrt{2} \sqrt{P}$. For constant relative intensity deviations ΔI_P this implies $const. = \frac{\sqrt{P^2}}{z_R^2} \cdot P^2$ or $z_R \propto P^{3/2}$. A numerical investigation, see Fig. 7, confirms $z_{\min}(P) = 2.2 \cdot \lambda_L \cdot P^{3/2}$ as a good estimate for a lower bound on z_R . This relationship has been checked numerically and holds for $7 < P < 30$. There is no reason to believe deviations might occur for values of $P > 30$, but

for small values of P the assumptions used in the derivation of the scaling law do not hold accurately, see Fig. 2. Instead, the expression $z_{\min}P = 15 \cdot \lambda_L \cdot P^{1/2}$ gives a better estimate for $z_{\min}P$ in the range of $0 < P \leq 6$. These lower limits for z_R imply that the beam focus is several wavelengths wide and a posteriori confirms that the paraxial approximations hold for all cases discussed here, since the largest beam opening angle conforming with the lower limits presented here turns out to be roughly 7° for superposition Ψ_2 .

V. CONCLUSIONS

For a possible experimental implementation of focussing fields repulsive (blue-detuned) optical potentials with a dark center are probably most suited since they minimize detrimental spontaneous emission noise. For an expansion field analogously red detuned optical potentials [9] should be used. If fine-tuning is considered one will probably also have to revisit the approximations underlying Eq. (4) and Eq. (6); such considerations are beyond the scope of this paper.

The techniques for the coherent superposition of laser modes have been experimentally demonstrated, see e.g. references [24, 30] and citations therein. We have found here that using the mode-superposition approach allows for very considerable laser power savings and potentials can be made wider than is possible with pure modes. We come to the conclusion that for the design of atomic potentials, based on the optical dipole force, it is possible and necessary to coherently superpose suitable laser modes in order to create wide high quality parabolic potentials.

-
- [1] D. Meschede and H. Metcalf, J. Phys. D: Appl. Phys. **36**, R17 (2003).
 - [2] T. Seideman, J. Chem. Phys. **107**, 10420 (1997).
 - [3] H. Stapelfeldt, H. Sakai, E. Constant, and P. B. Corkum, Phys. Rev. Lett. **79**, 2787 (1997).
 - [4] I. Bloch, T. W. Hänsch, and T. Esslinger, Phys. Rev. Lett. **82**, 3008 (1999).
 - [5] J. Notte, B. Ward, N. Economou, R. Hill, R. Percival, L. Farkas, and S. McVey, in *Characterization and Metrology for Nanoelectronics*, edited by D. G. Seiler, A. C. Diebold, R. McDonald, M. C. Garner, D. Herr, R. P. Khosia, and E. M. Secula (2007), vol. 931 of *American Institute of Physics Conference Series*, pp. 489–496.

- [6] H. Marion, F. Pereira Dos Santos, M. Abgrall, S. Zhang, Y. Sortais, S. Bize, I. Maksimovic, D. Calonico, J. Grünert, C. Mandache, et al., *Phys. Rev. Lett.* **90**, 150801 (2003).
- [7] M. Greiner, O. Mandel, T. Esslinger, T. W. Hänsch, and I. Bloch, *Nature* **415**, 39 (2002).
- [8] M. Greiner, C. A. Regal, and D. S. Jin, *Nature* **426**, 537 (2003).
- [9] T. Jelten, J. M. McNamara, W. Hogervorst, W. Vassen, V. Krachmalnicoff, M. Schellekens, A. Perrin, H. Chang, D. Boiron, A. Aspect, et al., *Nature* **445**, 402 (2007).
- [10] I. Bloch, J. Dalibard, and W. Zwerger, *Rev. Mod. Phys.* **80**, 885 (2008).
- [11] M. Jeppesen, J. Dugué, G. R. Dennis, M. T. Johnsson, C. Figl, N. P. Robins, and J. D. Close, *Phys. Rev. A* **77**, 063618 (2008).
- [12] O. Steuernagel, *Phys. Rev. A* **79**, 013421 (2009).
- [13] T. Miossec, R. Barbé, J.-C. Keller, and O. Gorceix, *Opt. Commun.* **209**, 349 (2002).
- [14] H. J. Metcalf and P. van der Straten, *Laser Cooling and Trapping* (Springer, New York, 1999).
- [15] O. Steuernagel, *J. Opt. A: Pure Appl. Opt.* **7**, S392 (2005), arXiv:physics/0502023.
- [16] J. Fortágh and C. Zimmermann, *Science* **307**, 860 (2005).
- [17] D. R. Murray and P. Öhberg, *J. Phys. B: At. Mol. Phys.* **38**, 1227 (2005).
- [18] N. Friedman, A. Kaplan, D. Carasso, and N. Davidson, *Phys. Rev. Lett.* **86**, 1518 (2001).
- [19] E. A. Cornell, C. Monroe, and C. E. Wieman, *Phys. Rev. Lett.* **67**, 2439 (1991).
- [20] E. A. Hinds and I. G. Hughes, *J. Phys. D: Appl. Phys.* **32**, R119 (1999).
- [21] E. Knyazchyan, B. Mercier, H. Perrin, P.-E. Pottie, and V. Lorent, *J. Phys. Conf. Ser.* **19**, 44 (2005).
- [22] A. S. Arnold, M. J. Pritchard, D. A. Smith, and I. G. Hughes, *New J. Phys.* **8**, 53 (2006).
- [23] U. Hohenester, A. Eiguren, S. Scheel, and E. A. Hinds, *Phys. Rev. A* **76**, 033618 (2007), 0707.0238.
- [24] C. Maurer, A. Jesacher, S. Fürhapter, S. Bernet, and M. Ritsch-Marte, *New J. Phys.* **9**, 78 (2007).
- [25] O. Steuernagel, *Am. J. Phys.* **73**, 625 (2005).
- [26] L. Allen, M. W. Beijersbergen, R. J. C. Spreeuw, and J. P. Woerdman, *Phys. Rev. A* **45**, 8185 (1992).
- [27] A. E. Siegman, *Lasers* (Oxford Univ. Press, Oxford, 1986).
- [28] H. A. Haus, *Electromagnetic Noise and Quantum Optical Measurements* (Springer, Heidelberg, 2000).

- [29] F. Pampaloni and J. Enderlein (2004), arXiv:physics/0410021.
- [30] O. Steuernagel, E. Yao, K. O'Holleran, and M. Padgett, *J. Mod. Opt.* **52**, 2713 (2005).
- [31] G. M. Gallatin and P. L. Gould, *J. Opt. Soc. Am. B* **8**, 502 (1991).
- [32] V. Natarajan, R. Behringer, and G. Timp, *Phys. Rev. A* **53**, 4381 (1996).
- [33] J. J. Hope and C. M. Savage, *Phys. Rev. A* **53**, 1697 (1996).
- [34] M. T. DePue, C. McCormick, S. L. Winoto, S. Oliver, and D. S. Weiss, *Phys. Rev. Lett.* **82**, 2262 (1999).